

Performance Analysis of RIS-Assisted Full-Duplex Communication over Correlated Nakagami- m Fading Channel

Tianxiong Wang, *Student Member, IEEE*, Gaojie Chen, *Senior Member, IEEE*,
and Justin P. Coon, *Senior Member, IEEE*,

Abstract—In this paper, we investigate the performance of a reconfigurable intelligent surface (RIS) assisted full-duplex (FD) communication network, where each user is facilitated by a specific RIS in the network. The correlated Nakagami- m fading channel is first considered in a RIS system, which is a general channel model that can capture the spatial correlation effect inherent in the RIS-assisted communication system. Using the two-dimensional Laplace transform and its inverse, the closed form expressions of the mean and variance of the signal power distribution are obtained. Then, the outage probability and average achievable rates of the uplink and downlink users are derived in closed form. Furthermore, the impact of the residual self-interference (SI) on FD communication performance is discussed. It is demonstrated that FD communication outperforms HD communication when the residual SI is below a threshold, and the threshold is derived in closed form. Simulation results are presented to confirm the accuracy of the theoretical analysis and show the negative impact of channel correlation on the system performance. Moreover, it is illustrated that the outage probability and the average achievable rate of the uplink user will converge to a constant when the residual SI is linearly dependent on the transmit power.

Index Terms—Reconfigurable intelligent surface (RIS), full-duplex (FD), channel correlation, Nakagami- m fading

I. INTRODUCTION

The upcoming wireless communication networks, including beyond fifth-generation (B5G) and sixth-generation (6G), are expected to provide ubiquitous wireless connectivity for billions of communication devices with high requirements in terms of data rates, latency, spectral and energy efficiency and reliability [1]. To meet these significant demands, various innovative physical layer wireless communication technologies have been explored and developed in the recent past, such as massive multiple-input multiple-output (MIMO)

[2], millimeter-wave (mm-wave) communications [3], ultra-reliable low latency communications (URLLC) [4], and network densification [5]. Among these potential technologies, reconfigurable intelligent surface (RIS) assisted wireless communication has gained enormous research interests and has been regarded as a promising physical layer technology in the future wireless communication networks, which can improve the spectral and energy efficiency of wireless communications with low hardware cost [6]. Specifically, a RIS is a planar array consisting of a large number of reflecting elements. With the development of metamaterials and metasurfaces, each element is controlled by the RIS controller to perform real-time independent phase shifting of the incident signals [7]. With the channel state information (CSI), a RIS is capable of reconfiguring the wireless propagation environment intelligently by adjusting the phase shifts of all the reflecting elements such that the signals can be combined constructively and destructively towards different directions to achieve spatial signal enhancement and nulling, thus enhancing the communication performance [8]. In addition, a RIS does not need the active radio frequency (RF) chains, which significantly reduces the hardware cost and energy consumption of RIS [9]. Owing to the above advantages, RIS has been investigated in various wireless networks. RIS-empowered orthogonal frequency division multiplexing (OFDM) and RIS-aided non-orthogonal multiple access (NOMA) were investigated in [10] and [11], respectively. The authors in [12] studied the physical layer security in a RIS-assisted wireless network, and the RIS-assisted UAV communication was explored in [13].

As a brand new technology, the performance of RIS-assisted uplink/downlink wireless communications has been studied extensively in various scenarios, where the performance gains brought by deploying RISs in these systems have been illustrated. The authors in [14] analyzed the path loss of a RIS-assisted wireless system and demonstrated the double fading effect such that the large-scale fading is inversely proportional to the product of the distances of the incident and reflecting channels. Over an independent Rayleigh fading channel model, the authors in [15] analyzed the outage probability, average achievable rate, and symbol error rate of a RIS-assisted downlink communication system with perfect phase alignment. With the same system model, an upper bound on the average achievable rate was given as a concise form in [16] and proved to be asymptotically equivalent in the number of reflecting elements. Considering

Copyright (c) 2015 IEEE. Personal use of this material is permitted. However, permission to use this material for any other purposes must be obtained from the IEEE by sending a request to pubs-permissions@ieee.org.

This research was funded in part by EPSRC grant number EP/T02612X/1. For the purpose of Open Access, the author has applied a CC BY public copyright licence to any Author Accepted Manuscript (AAM) version arising from this submission.

T. Wang is with the Department of Engineering Science, University of Oxford, Oxford, OX1 3PJ, U.K. He is also with the Future Research Laboratory, China Mobile Research Institute, Beijing, 100053, China. (e-mail: tianxiong.wang@eng.ox.ac.uk).

G. Chen is with 5GIC & 6GIC, Institute for Communication Systems (ICS), University of Surrey, Guildford, GU2 7XH, U.K. (e-mail: gaojie.chen@surrey.ac.uk).

J. P. Coon is with the Department of Engineering Science, University of Oxford, Oxford, OX1 3PJ, U.K. (e-mail: justin.coon@eng.ox.ac.uk).

the phase quantization errors, the authors in [17] analyzed the outage probability and diversity order of a RIS-assisted communication system with a 1-bit phase adjustment scheme. As a step further, the authors in [18] derived the symbol error rate and diversity order with the general phase errors pattern by using the central limit theorem (CLT) and proved that the composite channel gain is Nakagami- m distributed. More general channel models, e.g., Rician fading and Nakagami- m fading, were considered in other works [19]–[23]. The authors in [19] derived an approximation and an upper bound of the outage probability and the ergodic capacity of a downlink RIS-assisted communication system over the independent Rician fading channel model, respectively. Under a similar system model, an asymptotic analysis was carried out in [20] to characterize the diversity order of the system. A discrete phase shifting scheme was considered in [21], where the authors derived the required phase shifting levels under a constraint on the capacity degradation. As a step further, the more general Nakagami- m fading channel model was adopted in some recent works. The authors in [22] analyzed the bit error probability of a RIS-assisted communication network over the independent Nakagami- m channel model with and without phase errors, respectively. The outage probability of a RIS-aided system over Nakagami- m channels was given in an integral form with the Gil-Pelaez theorem in [23]. It is worth noting that all the above works considered independent channel models. However, channel correlation is inevitable in RIS systems since all the sub-wavelength reflecting elements are closely compacted together in a rectangular array [24]. Therefore, the correlated channel model is more reasonable in RIS systems. The authors in [25] and [26] analyzed the outage probability of a RIS-assisted communication scheme over correlated Rayleigh fading channels with optimal and random phase shifting schemes, respectively. With a similar system model, an upper bound on the average achievable rate was proposed in [27]. Applying the equal correlation profile, the authors in [28] investigated the outage probability and diversity order of a RIS system with a correlated Rician fading channel model. Moreover, the authors in [29] explored the uplink single-input multiple-output (SIMO) scenario and characterized the optimal signal-to-noise ratio (SNR) over correlated Rician fading channels.

To improve the spectral efficiency of wireless communications, full-duplex (FD) communication technology is regarded as another promising wireless communications technology. Contrary to the conventional half-duplex (HD) system, the FD system enables signal transmission and reception with the same time and frequency resource block, thus boosting spectral efficiency. Therefore, significant research efforts have been devoted to RIS-assisted FD communication to characterize the performance of the combination of these two spectral efficient techniques. The authors in [30] proposed a RIS-assisted FD MIMO communication system and maximized the sum rate by jointly optimizing the beamforming vectors at users and the phase shifting matrix at the RIS. The outage probability, diversity order, and spectral efficiency of a RIS-

aided FD communication system over independent Rayleigh fading channels were derived in closed form in [31]. The authors in [32] proposed a RIS-assisted FD system, where an FD transceiver simultaneously serves a downlink user and an uplink user over the same frequency band. The total power consumption was minimized by jointly optimizing the transmit power of uplink and downlink transmissions and the reflecting coefficients of the RISs. The authors in [33] analyzed the performance of an FD communication system over independent Nakagami- m fading channel models, where an FD transceiver communicates with a downlink user and an uplink user with the aid of two separate RISs in the FD mode. Considering the external interference from jammers, the authors in [34] derived the outage probability and ergodic capacity of a RIS-assisted FD communication system over Weibull fading channels when the RIS conducts the random phase shifting scheme. The authors in [35] characterized the performance degradation due to channel estimation and phase quantization errors of a RIS-assisted FD system over independent Rayleigh fading channels. The authors in [36] proposed a RIS-assisted FD communication system where two RISs were deployed to serve two end users separately, and the channels were Nakagami- m fading. Outage probability and symbol error probability were then derived in closed form. Following a similar system model, the authors in [37] considered the correlated Rayleigh fading channel model and demonstrated the impact of channel correlation on the system performance. Although the correlated Rayleigh fading channel model has been studied, it can only capture the rich scattering propagation environment without LoS link. The correlated Nakagami- m fading channel model is a more general and accurate channel model for multiple propagation environments, thus it requires more investigation and remains untouched so far.

To fill the research gap, this paper presents novel results regarding the RIS-assisted FD communication system with correlated Nakagami- m fading channels. The main contributions of this paper are listed below:

- 1) We study a RIS-assisted FD communication network, where an FD transceiver communicates with a downlink user and an uplink user simultaneously within the same frequency band. Two RISs are set to individually serve the uplink user and the downlink user. The channels associated with the RISs are assumed as correlated Nakagami- m fading. Both the inter-user interference and the residual self-interference (SI) are considered.
- 2) Exact closed form expressions for the mean and variance of the signal power expressions are derived in terms of elementary and special functions by using the definition of Nakagami- m distribution and the two-dimensional Laplace transform, leading to approximations to the distributions of the received signal to interference plus noise ratio (SINR) of different users. Then, the outage probability and the average achievable rates of the uplink and downlink transmissions are obtained in

closed form. With the derived expressions, the residual SI threshold below which the FD communication outperforms the HD counterpart is given, and the impact of the residual SI exponent on the performance of the uplink transmission is also investigated.

- 3) Numerical results are presented to confirm the effectiveness of the analysis. Channel correlation will lead to higher outage probability and lower average achievable rates compared to the benchmark of uncorrelated channels. Furthermore, FD communication can perform better than HD communication only when the residual SI is below the given threshold. In the case that the uplink user and the FD transceiver have the same transmit power, and the residual SI is linearly dependent on the transmit power, the uplink performance metrics will converge to constants in the large transmit power regime.

The rest of the paper is organized as follows. Section II introduced the system model. The outage probability of the uplink and downlink transmissions are analyzed in Section III. Section IV gives the average achievable rates of the uplink and downlink users, and discusses the impact of the residual SI on the FD communication. Section V presents the numerical results to verify the theoretical analysis, followed by Section VI to conclude the paper.

Notations: $\text{mod}(x, y)$ and $\lfloor x \rfloor$ stand for the remainder of x divided by y and the greatest integer less or equal to x ; $\mathbb{C}^{N \times 1}$ represents the space of the $N \times 1$ complex vectors; Nakagami(m, Ω) is the Nakagami- m distribution of shape parameter m and scale parameter Ω ; $\mathbb{E}[X]$, $\text{Var}(X)$ and $\text{Cov}(X, Y)$ denote the expectation of a random variable X , variance of X , and the covariance of X and Y ; ${}_2F_1(\cdot, \cdot; \cdot; \cdot)$, $\Gamma(\cdot)$ and $\gamma(\cdot, \cdot)$ are the hypergeometric function, gamma function and the lower incomplete gamma function, respectively. $\mathcal{CN}(\mu, \sigma^2)$ represents the complex Gaussian distribution of mean μ and variance σ^2 ; \mathbf{X}^T is the transpose of matrix \mathbf{X} .

II. SYSTEM MODEL

In this paper, we study a RIS-assisted FD wireless communication network in which an uplink (UL) user U_A and a downlink (DL) user U_B are served by a transceiver (TX) simultaneously. U_A and U_B are equipped with a single transmit antenna and a single receive antenna respectively, while TX has two antennas, one each for signal transmission and reception, operating in the FD mode¹. Since both users are assumed to be cell-edge users, two RISs, S_A and S_B , are deployed in close proximity to U_A and U_B respectively for improving the wireless propagation environment by tuning the phases of the corresponding channels. As shown in Fig. 1, the

¹Analysis of the multi-antenna scenarios will be studied in future work. Jointly designing active and passive beamforming schemes will be explored, which will then be used to carry out a performance analysis. However, the hardware limitations may prevent multi-antenna setups from being implemented in some scenarios. In such cases, the cost-effective wireless communication architecture using RIS-assisted communications with single-antenna TXs and users is particularly beneficial and useful. Many related works, such as [31], [37], [38], have discussed the potential of this approach.

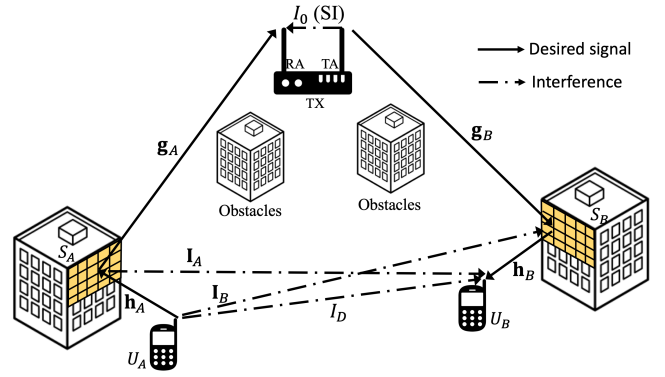


Fig. 1. System model of RIS-assisted FD communication system.

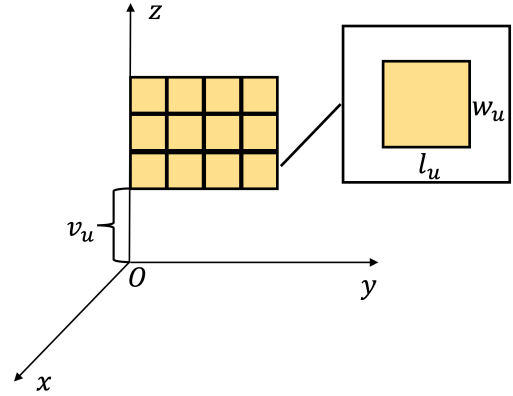


Fig. 2. RIS structure.

direct links between TX and users are assumed to be absent due to obstacles, large path loss and/or shadowing effect. The proposed system model can be generalized to the multi-user scenario with multiple users on both uplink and downlink by using the time division multiple access (TDMA) transmission scheme. In each time slot, TX serves a downlink user and an uplink user in the FD mode. In different time slots, TX serves different downlink and uplink users. The analysis in this paper can be regarded as a RIS-assisted FD TDMA system in a specific time slot.

A. RIS Structure

Two RISs are placed near their corresponding users to enhance the communication performance. S_u , $u \in \{A, B\}$ contains $M_u = M_{v,u}M_{h,u}$ elements equipped as a rectangular array, where $M_{v,u}$ and $M_{h,u}$ are the number of elements along the vertical and horizontal directions, respectively. Each element of S_u is of the dimension of $A_u = l_u \times w_u$ with l_u and w_u denoting the length and width of each element on S_u , respectively. As shown in Fig. 2, S_u is set on the yOz plane of height v_u . Therefore, the coordinate of the m th element of S_u is given as

$$\mathbf{c}_{m,u} = [0, l_u y_u(m), w_u z_u(m) + v_u], \quad m \in \{1, 2, \dots, M_u\}, \quad (1)$$

where

$$y_u(m) = \text{mod}(m-1, M_{h,u}), \quad z_u(m) = \lfloor \frac{m-1}{M_{h,u}} \rfloor. \quad (2)$$

$y_u(m)$ and $z_u(m)$ denote the y and z indexes of the m th element of S_u , respectively.

Assuming that each element of S_u is able to perform independent passive phase shifting without energy dissipation, the passive beamforming matrix of S_u can be given as

$$\Theta_u = \text{diag}(e^{j\theta_{1,u}}, \dots, e^{j\theta_{M_u,u}}), \quad (3)$$

where $\theta_{m,u}$, $m \in \{1, 2, \dots, M_u\}$ is the phase shift angle of the m th element of S_u .

B. Channel Model

1) *Small Scale Fading*: Let $\mathbf{h}_u = (h_{1,u}, \dots, h_{M_u,u})^T \in \mathbb{C}^{M_u \times 1}$, $\mathbf{g}_u = (g_{1,u}, \dots, g_{M_u,u})^T \in \mathbb{C}^{M_u \times 1}$ and $\mathbf{I}_u = (I_{1,u}, \dots, I_{M_u,u})^T \in \mathbb{C}^{M_u \times 1}$ represent the normalized small scale fading of the S_u - U_u , S_u -TX and S_u - $U_{u'}$ channels, respectively, where $u \in \{A, B\}$ and $u' \in \{A, B\} \setminus u$. Both RISs work in the far field of TX and users. In this paper, the correlated Nakagami- m fading model is applied. It is worth highlighting that the Nakagami- m fading is a general channel fading model which can model many types of distributions in wireless communications by adjusting the shape parameter, and Rayleigh fading is a special case of Nakagami- m fading with the unit shape parameter [39]. Specifically,

$$|h_{m,u}| \sim \text{Nakagami}(a_{h,u}, 1), \quad (4a)$$

$$|g_{m,u}| \sim \text{Nakagami}(a_{g,u}, 1), \quad (4b)$$

$$|I_{m,u}| \sim \text{Nakagami}(a_{I,u}, 1), \quad (4c)$$

where $m \in \{1, \dots, M_u\}$; $a_{h,u}$, $a_{g,u}$ and $a_{I,u}$ are the shape parameters of the corresponding channels. $|h_{m,u}|$, $|g_{m,u}|$ and $|I_{m,u}|$ have the same unit scale parameters. The channel correlation is characterized by the well-known exponential decay power correlation model as introduced in many relative literatures such as [40]–[42]. Under this model, for the channel S_u - U_u , we can have the power correlation coefficient of $|h_{m,u}|$ and $|h_{n,u}|$ where $m, n \in \{1, 2, \dots, M_u\}$ as

$$\rho_{m,n,u} = \frac{\text{Cov}(|h_{m,u}|^2, |h_{n,u}|^2)}{\sqrt{\text{Var}(|h_{m,u}|^2) \text{Var}(|h_{n,u}|^2)}} = \rho_u \frac{\|\mathbf{c}_{m,u} - \mathbf{c}_{n,u}\|}{c_{0,u}}, \quad (5)$$

where $0 < \rho_u < 1$ is the power correlation coefficient of the channels associated with the nearest neighboring elements on S_u ; $\|\mathbf{c}_{m,u} - \mathbf{c}_{n,u}\|$ is the distance between the m th and n th elements on S_u ; $c_{0,u}$ is the smallest element spacing of S_u . Under the same framework, it can be learned that (5) also applies to the power correlation coefficients of $|g_{m,u}|$ and $|g_{n,u}|$, as well as $|I_{m,u}|$ and $|I_{n,u}|$, such that

$$\begin{aligned} \rho_{m,n,u} &= \frac{\text{Cov}(|g_{m,u}|^2, |g_{n,u}|^2)}{\sqrt{\text{Var}(|g_{m,u}|^2) \text{Var}(|g_{n,u}|^2)}} \\ &= \frac{\text{Cov}(|I_{m,u}|^2, |I_{n,u}|^2)}{\sqrt{\text{Var}(|I_{m,u}|^2) \text{Var}(|I_{n,u}|^2)}}. \end{aligned} \quad (6)$$

The exponential decay power correlated Nakagami- m fading channel model can be reduced to the correlated Rayleigh fading channel model by setting the shape parameter as one.

The normalized small scale fading of the U_A - U_B channel and the SI channel from the transmit antenna (TA) to the receive antenna (RA) at TX are denoted as I_D and I_0 , respectively. I_D is circularly symmetric complex Gaussian (CSCG) distributed with unit power such that $I_D \sim \mathcal{CN}(0, 1)$, thus $|I_D|$ is Rayleigh distributed, i.e., $|I_D| \sim \mathcal{R}(\sqrt{2}/2)$.

It is assumed that S_A and S_B are sufficiently far from U_B and U_A , respectively [37]. Furthermore, U_A and U_B are assumed to be two cell-edge users assisted by RISs which are in sufficiently long distances to TX [6]. Therefore, the channel that S_A reflects the signal from TX to U_B , the channel that S_B reflects the signal from U_A to TX, and the channel that S_B reflects back the signal from TX to itself can be ignored due to the long distances [32].

2) *Path Loss*: The path loss of the U_u - S_u -TX, U_A - S_u - U_B and U_A - U_B channels, where $u \in \{A, B\}$, can be given respectively as [43]

$$\eta_u = \frac{\Lambda_u}{d_{h,u}^\chi d_{g,u}^\chi}, \quad \eta_{I,u} = \frac{\Lambda_{I,u}}{d_{h,u}^\chi d_{I,u}^\chi}, \quad \eta_D = \frac{\Lambda_D}{d_0^\chi}. \quad (7)$$

where Λ_u , $\Lambda_{I,u}$ and Λ_D are the path loss per unit distance of the U_u - S_u -TX, U_A - S_u - U_B and U_A - U_B channels, respectively; $d_{h,u}$, $d_{g,u}$, $d_{I,u}$ and d_0 denote respectively the distances of the S_u - U_u , S_u -TX, S_u - $U_{u'}$ and U_A - U_B links, where $u \in \{A, B\}$ and $u' \in \{A, B\} \setminus u$; χ stands for the path loss exponent. The position of the RIS affects the path loss of the corresponding channel. The path loss is inversely proportional to the product of the distances of the TX-RIS and the RIS-user channels. The larger the product, the more serious the path loss.

C. Signal Model

The received signal at TX from the uplink transmission and received by U_B from the downlink transmission are introduced separately. The received signal at TX can be given as

$$y_T = \mathbf{g}_A^T \Theta_A \mathbf{h}_A \sqrt{P_A \eta_A} s_A + I_0 \sqrt{P_T} s_T + n_T, \quad (8)$$

where the first term and the second term refer to the desired signal and the SI, respectively; P_A and P_T are the transmit power of U_A and TX, respectively; s_A and s_T are the independent transmit constellation symbols of U_A and TX with unit power such that $\mathbb{E}[|s_A|^2] = \mathbb{E}[|s_T|^2] = 1$ and $\mathbb{E}[s_A s_T] = 0$; $n_T \sim \mathcal{CN}(0, \sigma_T^2)$ is the additive white Gaussian noise (AWGN) with zero mean and variance σ_T^2 . Similar to [36] and [37], it is assumed that S_A only has the channel state information (CSI) of the channels² associated with its pairing user U_A , which are \mathbf{g}_A and \mathbf{h}_A . Therefore, the phase shift of each element on S_A is adjusted to co-phase the reflecting links such that

$$\theta_{m,A} = -\arg(g_{m,A}) - \arg(h_{m,A}), \quad m \in \{1, 2, \dots, M_A\}. \quad (9)$$

²This paper assumes the accurate channel estimation, thus it gives upper bounds of the actual system performance. The impacts of inaccurate channel estimation and imperfect CSI will be considered in future works.

After proper phase shifting, the received signal at TX can be rewritten as

$$y_T = H_A \sqrt{P_A \eta_A} s_A + I_0 \sqrt{P_T} s_T + n_T, \quad (10)$$

where

$$H_A = \sum_{m=1}^{M_A} |g_{m,A}| |h_{m,A}|. \quad (11)$$

Thus, the received SINR of the uplink transmission from U_A to TX can be given as

$$\gamma_A = \frac{P_A \eta_A H_A^2}{P_T |I_0|^2 + \sigma_T^2}. \quad (12)$$

In practice, several SI cancellation techniques can be applied to alleviate the SI and lead to the residual SI [44]. Among difference frameworks used in existing works to model the residual SI for FD communication, in this paper, we adopt the model where the residual SI is subject to a Gaussian random variable with zero mean and variance σ_l^2 [45]. The variance depends on the transmit power and is modeled as

$$\sigma_l^2 = \varpi P_T^\epsilon, \quad (13)$$

where the two parameters, $\varpi > 0$ and $\epsilon \in [0, 1]$, depend on the SI cancellation method used at TX [46]. After several stages of SI cancellation, the received SINR of TX can be rewritten as

$$\gamma_A = \frac{P_A \eta_A H_A^2}{\sigma_l^2 + \sigma_T^2}. \quad (14)$$

The received signal at U_B can be expressed as

$$y_B = \mathbf{h}_B^T \mathbf{\Theta}_B \mathbf{g}_B \sqrt{P_T \eta_B} s_T + \tilde{I} \sqrt{P_A} s_A + n_B, \quad (15)$$

where

$$\tilde{I} = \sqrt{\eta_{I,A}} \mathbf{I}_A^T \mathbf{\Theta}_A \mathbf{h}_A + \sqrt{\eta_{I,B}} \mathbf{h}_B^T \mathbf{\Theta}_B \mathbf{I}_B + \sqrt{\eta_D} I_D, \quad (16)$$

in which the first and second terms denote the interference from U_A reflected by S_A and S_B , respectively; the third term stands for the interference from U_A transmitted through the direct link. $n_B \sim \mathcal{CN}(0, \sigma_B^2)$ is the additive white Gaussian noise (AWGN) with zero mean and variance σ_B^2 . Similar to S_A , S_B can only obtain the CSI of the channels \mathbf{g}_B and \mathbf{h}_B which are the signal transmission channels regarding its pairing user U_B , and the phase shifts of elements on S_B are controlled to boost the signal transmission through the channel TX- S_B - U_B , i.e.,³

$$\theta_{m,B} = -\arg(g_{m,B}) - \arg(h_{m,B}), \quad m \in \{1, 2, \dots, M_B\}. \quad (17)$$

After phase shifting, the received signal at U_B can be rewritten as

$$y_B = H_B \sqrt{P_T \eta_B} s_T + \tilde{I} \sqrt{P_A} s_A + n_B, \quad (18)$$

³This paper assumes the ideal coherent phase shifting, thus it gives upper bounds of the actual performance due to the phase errors. Further, only 2-bit phase adjustment can already achieve the nearly optimal performance [17].

where

$$H_B = \sum_{m=1}^{M_B} |h_{m,B}| |g_{m,B}|, \quad (19a)$$

$$\begin{aligned} \tilde{I} = & \sqrt{\eta_{I,A}} \sum_{m=1}^{M_A} |I_{m,A}| |h_{m,A}| e^{j\phi_{m,A}} \\ & + \sqrt{\eta_{I,B}} \sum_{m=1}^{M_B} |h_{m,B}| |I_{m,B}| e^{j\phi_{m,B}} \\ & + \sqrt{\eta_D} |I_D| e^{j\phi_D}. \end{aligned} \quad (19b)$$

Since the channels \mathbf{h}_u , \mathbf{g}_u and \mathbf{I}_u , $u \in \{A, B\}$ are independent with each other, and the phase shifts of S_A and S_B are manipulated respectively to boost the U_A - S_A -TX and TX- S_B - U_B channels, it can be learned that $\phi_{m,u}$, $u \in \{A, B\}$, $m \in \{1, 2, \dots, M_u\}$, are independent and identically distributed (i.i.d.) random variables which follow the uniform distribution over $[-\pi, \pi)$. Further, due to the distribution of I_D , ϕ_D is also uniformly distributed over $[-\pi, \pi)$. Hence, the SINR of U_B can be given as

$$\gamma_B = \frac{P_T \eta_B H_B^2}{P_A I + \sigma_B^2}, \quad (20)$$

where $I = |\tilde{I}|^2$.

D. Performance Metrics

In this paper, we analyze the outage probability and the ergodic capacity of the uplink and downlink transmissions.

1) *Outage Probability*: Outage probability is a performance metric to characterize the reliability of wireless communication. It is the probability that the received SINR falls below a threshold, i.e.,

$$\bar{P}_u(\bar{\gamma}) = \mathbb{P}(\gamma_u < \bar{\gamma}), \quad u \in \{A, B\}, \quad (21)$$

where $\bar{\gamma}$ is the SINR threshold.

2) *Ergodic Capacity*: Ergodic capacity is a performance metric to evaluate the efficiency of wireless communication, and it is defined as

$$\begin{aligned} R_u = & \mathbb{E}[\log_2(1 + \gamma_u)] \\ = & \int_0^\infty \log_2(1 + x) f_{\gamma_u}(x) dx, \quad u \in \{A, B\}, \end{aligned} \quad (22)$$

where $f_{\gamma_u}(x)$ denotes the PDF of γ_u .

III. OUTAGE PROBABILITY ANALYSIS

In this section, we analyze the outage probability of UL user U_A and DL user U_B , respectively. The distribution of the composite channel gain H_u , $u \in \{A, B\}$ is characterized first, followed by deriving the outage probability expressions of the two users.

A. Channel Distribution Analysis

The random variable H_u , $u \in \{A, B\}$ is the sum of products of correlated Nakagami- m random variables. The exact statistical characterization of H_u is mathematically intractable. Therefore, in this case, we analyzed the mean and variance of H_u first, based on which the distribution of H_u is fitted by a gamma random variable. The gamma distribution is often applied to fit some sophisticated distributions due to its advantages in terms of convenient parameter calculations and high accuracy [47]. Therefore, we derive the mean and variance of H_u in the following proposition.

Proposition 1. *The mean and variance of H_u , $u \in \{A, B\}$ can be given as*

$$\begin{aligned} \mathbb{E}[H_u] &= \sum_{m=1}^{M_u} \mathbb{E}[|h_{m,u}|] \mathbb{E}[|g_{m,u}|] \\ &= M_u \frac{\Gamma(a_{h,u} + \frac{1}{2}) \Gamma(a_{g,u} + \frac{1}{2})}{\Gamma(a_{h,u}) \Gamma(a_{g,u})} \left(\frac{1}{a_{h,u} a_{g,u}} \right)^{\frac{1}{2}}, \end{aligned} \quad (23a)$$

$$\begin{aligned} \text{Var}[H_u] &= \sum_{m=1}^{M_u} \sum_{n=1}^{M_u} [\mathbf{R}_{h,u}]_{m,n} [\mathbf{R}_{g,u}]_{m,n} \\ &\quad - \frac{M_u^2}{a_{h,u} a_{g,u}} \left(\frac{\Gamma(a_{h,u} + \frac{1}{2}) \Gamma(a_{g,u} + \frac{1}{2})}{\Gamma(a_{h,u}) \Gamma(a_{g,u})} \right)^2, \end{aligned} \quad (23b)$$

where

$$\mathbf{R}_{h,u} = \mathbb{E}[|\mathbf{h}_u| |\mathbf{h}_u|^T], \quad (24a)$$

$$\mathbf{R}_{g,u} = \mathbb{E}[|\mathbf{g}_u| |\mathbf{g}_u|^T]; \quad (24b)$$

each elements of $\mathbf{R}_{h,u}$ and $\mathbf{R}_{g,u}$ are respectively given as

$$\begin{aligned} [\mathbf{R}_{h,u}]_{m,n} &= \mathbb{E}[|h_{m,u}| |h_{n,u}|] \\ &= \frac{\Gamma^2(a_{h,u} + \frac{1}{2})}{a_{h,u} \Gamma^2(a_{h,u})} {}_2F_1 \left(-\frac{1}{2}, -\frac{1}{2}, a_{h,u}, \rho_{m,n,u} \right), \end{aligned} \quad (25a)$$

$$\begin{aligned} [\mathbf{R}_{g,u}]_{m,n} &= \mathbb{E}[|g_{m,u}| |g_{n,u}|] \\ &= \frac{\Gamma^2(a_{g,u} + \frac{1}{2})}{a_{g,u} \Gamma^2(a_{g,u})} {}_2F_1 \left(-\frac{1}{2}, -\frac{1}{2}, a_{g,u}, \rho_{m,n,u} \right). \end{aligned} \quad (25b)$$

Proof: See Appendix A. \square

Remark 1. *When the channels are uncorrelated, the mean and variance of H_u , $u \in \{A, B\}$ can be derived directly as*

$$\mathbb{E}[H_u] = M_u \frac{\Gamma(a_{h,u} + \frac{1}{2}) \Gamma(a_{g,u} + \frac{1}{2})}{\Gamma(a_{h,u}) \Gamma(a_{g,u})} \left(\frac{1}{a_{h,u} a_{g,u}} \right)^{\frac{1}{2}}, \quad (26a)$$

$$\text{Var}[H_u] = M_u - \frac{M_u}{a_{h,u} a_{g,u}} \left(\frac{\Gamma(a_{h,u} + \frac{1}{2}) \Gamma(a_{g,u} + \frac{1}{2})}{\Gamma(a_{h,u}) \Gamma(a_{g,u})} \right)^2. \quad (26b)$$

Remark 2. *Even though the exponential decay power correlation model is adopted in this paper, the proposed method can be generalized to other correlation profiles, such as the equal correlation model [48].*

With the mean and variance of H_u , $u \in \{A, B\}$, we can use the moment-matching method to fit the distribution of H_u to a gamma distribution, of which the shape parameter κ_u and the scale parameter ω_u are provided as follows:

$$\kappa_u = \frac{\mathbb{E}^2[H_u]}{\text{Var}[H_u]}, \quad \omega_u = \frac{\text{Var}[H_u]}{\mathbb{E}[H_u]}. \quad (27)$$

Hence, the PDF and CDF of H_u can be written as

$$f_{H_u}(x) = \frac{x^{\kappa_u-1} \exp(-x/\omega_u)}{\Gamma(\kappa_u) \omega_u^{\kappa_u}}, \quad (28a)$$

$$F_{H_u}(x) = \frac{\gamma(\kappa_u, x/\omega_u)}{\Gamma(\kappa_u)}. \quad (28b)$$

B. Outage Probability of UL and DL Users

1) *Outage Probability of U_A :* The outage probability of U_A can be expressed as

$$\begin{aligned} \bar{P}_A(\bar{\gamma}) &= \mathbb{P}(\gamma_A < \bar{\gamma}) \\ &= \mathbb{P}\left(\frac{P_A \eta_A H_A^2}{\sigma_l^2 + \sigma_T^2} < \bar{\gamma}\right) \\ &= F_{H_A}\left(\sqrt{\frac{\bar{\gamma}(\sigma_l^2 + \sigma_T^2)}{P_A \eta_A}}\right) \end{aligned} \quad (29)$$

Since the CDF of H_A has been given in (28b), the outage probability of U_A is written as

$$\bar{P}_A(\bar{\gamma}) = \frac{1}{\Gamma(\kappa_A)} \gamma\left(\kappa_A, \sqrt{\frac{\bar{\gamma}(\sigma_l^2 + \sigma_T^2)}{P_A \eta_A \omega_A^2}}\right). \quad (30)$$

Remark 3. *Considering the case of $P_A = P_T$, the impact of the residual SI on the outage probability depends on the residual SI exponent ϵ . If $0 \leq \epsilon < 1$, the outage probability will decrease with the increase of P_A , and smaller ϵ will lead to lower outage probability; If $\epsilon = 1$ and P_A is large, the outage probability will be independent with P_A , such that*

$$\bar{P}_A(\bar{\gamma}) = \frac{1}{\Gamma(\kappa_A)} \gamma\left(\kappa_A, \sqrt{\frac{\bar{\gamma} \omega}{\eta_A \omega_A^2}}\right). \quad (31)$$

2) *Outage Probability of U_B :* As per the expressions of the received SINR of U_B and the CDF of H_B , the outage

probability of U_B is computed as

$$\begin{aligned}
\bar{P}_B(\bar{\gamma}) &= \mathbb{P}(\gamma_B < \bar{\gamma}) \\
&= \mathbb{P}\left(\frac{P_T \eta_B H_B^2}{P_A I + \sigma_B^2} < \bar{\gamma}\right) \\
&= \int_0^\infty F_{H_B}\left(\sqrt{\frac{\bar{\gamma}(P_A x + \sigma_B^2)}{P_T \eta_B}}\right) f_I(x) dx \\
&= \int_0^\infty \frac{1}{\Gamma(\kappa_B)} \gamma \left(\kappa_B, \sqrt{\frac{\bar{\gamma}(P_A x + \sigma_B^2)}{P_T \eta_B \omega_B^2}}\right) f_I(x) dx.
\end{aligned} \tag{32}$$

To further simplify the outage probability of U_B , it is required to figure out the distribution of I , which is summarized in the following proposition.

Proposition 2. *The aggregate interference power I approximately follows the exponential distribution with the distribution parameter*

$$\xi_I = \frac{1}{\eta_{I,A} M_A + \eta_{I,B} M_B + \eta_D} \tag{33}$$

Hence, the PDF and CDF of I can be given as

$$f_I(x) = \xi_I e^{-\xi_I x}, \quad F_I(x) = 1 - e^{-\xi_I x}. \tag{34}$$

Proof: According to the system model, the aggregate interference power I is written as

$$I = |\tilde{I}|^2 = \left| \sqrt{\eta_{I,A}} \tilde{I}_A + \sqrt{\eta_{I,B}} \tilde{I}_B + \sqrt{\eta_D} I_D \right|^2, \tag{35}$$

where

$$\tilde{I}_A = \sum_{m=1}^{M_A} |I_{m,A}| |h_{m,A}| e^{j\phi_{m,A}}, \tag{36a}$$

$$\tilde{I}_B = \sum_{m=1}^{M_B} |I_{m,B}| |h_{m,B}| e^{j\phi_{m,B}}. \tag{36b}$$

The distribution of \tilde{I}_A is characterized first. Since $\phi_{m,A}$ follows the uniform distribution within $(-\pi, \pi]$, the expectation and variance of $|I_{m,A}| |h_{m,A}| \cos(\phi_{m,A})$ and $|I_{m,A}| |h_{m,A}| \sin(\phi_{m,A})$ are derived as

$$\begin{aligned}
\mathbb{E}[|I_{m,A}| |h_{m,A}| \cos(\phi_{m,A})] \\
= \mathbb{E}[|I_{m,A}| |h_{m,A}| \sin(\phi_{m,A})] = 0,
\end{aligned} \tag{37a}$$

$$\begin{aligned}
\text{Var}[|I_{m,A}| |h_{m,A}| \cos(\phi_{m,A})] \\
= \text{Var}[|I_{m,A}| |h_{m,A}| \sin(\phi_{m,A})] = \frac{1}{2}.
\end{aligned} \tag{37b}$$

Moreover, these two terms are proved to be uncorrelated with each other due to the relation:

$$\begin{aligned}
\mathbb{E}[|I_{m,A}|^2 |h_{m,A}|^2 \cos(\phi_{m,A}) \sin(\phi_{m,A})] \\
= \mathbb{E}[|I_{m,A}| |h_{m,A}| \cos(\phi_{m,A})] \mathbb{E}[|I_{m,A}| |h_{m,A}| \sin(\phi_{m,A})].
\end{aligned} \tag{38}$$

Hence, with the CLT, \tilde{I}_A can be approximated as a CSCG random variable with zero mean and variance M_A , such that

$$\tilde{I}_A \sim \mathcal{CN}(0, M_A). \tag{39}$$

Following the same method, we can obtain that \tilde{I}_B also follows the CSCG distribution with zero mean and variance M_B , i.e.,

$$\tilde{I}_B \sim \mathcal{CN}(0, M_B). \tag{40}$$

Since I_D is also CSCG distributed and applying the property of the sum of CSCG random variables, we can obtain the distribution of \tilde{I} as

$$\tilde{I} \sim \mathcal{CN}(0, \eta_{I,A} M_A + \eta_{I,B} M_B + \eta_D). \tag{41}$$

Recalling the relationship between exponential and CSCG distributions, we can arrive at the conclusion given in Proposition 2. \square

With the conclusion in Proposition 2, the outage probability of U_B can be rewritten as

$$\bar{P}_B(\bar{\gamma}) = \int_0^\infty \frac{\xi_I}{\Gamma(\kappa_B)} \gamma \left(\kappa_B, \sqrt{\frac{\bar{\gamma}(P_A x + \sigma_B^2)}{P_T \eta_B \omega_B^2}}\right) e^{-\xi_I x} dx. \tag{42}$$

The above integral can be evaluated numerically in efficient ways. On the other hand, we propose to use the Gaussian Chebyshev quadrature (GCQ) method to approximate (42), and derive an accurate closed form expression, which is provided in the following proposition.

Proposition 3. *Using the GCQ method, an approximation to the outage probability of U_B can be given in closed form as*

$$\begin{aligned}
\bar{P}_B^+(\bar{\gamma}) &= \frac{\pi}{2K\Gamma(\kappa_B)} \\
&\times \sum_{k=1}^K \sqrt{1 - \varphi_k^2} \gamma \left(\kappa_B, \sqrt{\frac{\bar{\gamma} \left(\frac{P_A}{\xi_I} \ln\left(\frac{1}{b_1}\right) + \sigma_B^2\right)}{P_T \eta_B \omega_B^2}}\right),
\end{aligned} \tag{43}$$

where

$$\varphi_k = \cos\left(\frac{\pi}{2K}(2k-1)\right), \tag{44a}$$

$$b_1 = \frac{\varphi_k}{2} + \frac{1}{2}; \tag{44b}$$

K is the complexity-accuracy trade-off factor, and the approximation error is negligible for large value of K .

Proof: Based on the integral form of the outage probability of U_B , by changing the integration variable of (42) as

$t = e^{-\xi_I x}$, we can obtain that

$$\begin{aligned} \bar{P}_B(\bar{\gamma}) &= \int_0^1 \frac{1}{\Gamma(\kappa_B)} \gamma \left(\kappa_B, \sqrt{\frac{\bar{\gamma} \left(\frac{P_A}{\xi_I} \ln \left(\frac{1}{t} \right) + \sigma_B^2 \right)}{P_T \eta_B \omega_B^2}} \right) dt \\ &\stackrel{(a)}{\approx} \frac{\pi}{2K\Gamma(\kappa_B)} \\ &\quad \times \sum_{k=1}^K \sqrt{1 - \varphi_k^2} \gamma \left(\kappa_B, \sqrt{\frac{\bar{\gamma} \left(\frac{P_A}{\xi_I} \ln \left(\frac{1}{b_1} \right) + \sigma_B^2 \right)}{P_T \eta_B \omega_B^2}} \right), \end{aligned} \quad (45)$$

where (a) follows from the GCQ method as introduced in [49]; φ_k and b_1 have been defined in (44a) and (44b), respectively. \square

Remark 4. The GCQ-based approximation is demonstrated to be highly accurate, even for small values of K . The relative error between $\bar{P}_B(\bar{\gamma})$ and $\bar{P}_B^+(\bar{\gamma})$ for different values of K is presented numerically in Section V.

IV. AVERAGE ACHIEVABLE RATE ANALYSIS

In this section, we characterize the average achievable rates of the uplink and downlink transmissions, respectively. Firstly, the approximate average achievable rates of U_A and U_B are derived by using the outage probability expressions of the two users obtained in the last section. Then, the performance of FD and HD communications are compared and discussed, relaying on upper bounds on the average achievable rates, which are in more concise form.

A. Approximate Average Achievable Rate Analysis

In the following lemma, the relationship between the outage probability and the average achievable rate is given.

Lemma 1. Assuming the outage probability of U_u , $u \in \{A, B\}$ is $\bar{P}_u(\bar{\gamma})$, where $\bar{\gamma}$ is the SINR threshold, the average achievable rate of U_u is given as

$$R_u = \frac{1}{\ln(2)} \int_0^\infty \frac{1 - \bar{P}_u(x)}{1 + x} dx. \quad (46)$$

Proof: See Appendix B. \square

1) *Average Achievable Rate of U_A :* With Lemma 1 and the outage probability expression given in (30), the average achievable rate of U_A can be written as

$$\begin{aligned} R_A &= \frac{1}{\ln(2)} \int_0^\infty \left(\frac{1}{1 + x} \right. \\ &\quad \left. - \frac{1}{(1 + x)\Gamma(\kappa_A)} \gamma \left(\kappa_A, \sqrt{\frac{x(\sigma_I^2 + \sigma_T^2)}{P_A \eta_A \omega_A^2}} \right) \right) dx \end{aligned} \quad (47)$$

Remark 5. Similar to the outage probability, if $P_A = P_T$, the impact of the residual SI on the average achievable rate depends on the residual SI exponent ϵ . If $0 \leq \epsilon < 1$, the average achievable rate will increase with the increase of

P_A , and smaller ϵ will lead to higher average achievable rate; If $\epsilon = 1$ and P_A is large, the average achievable will be independent with P_A , such that

$$\begin{aligned} R_A &= \frac{1}{\ln(2)} \int_0^\infty \left(\frac{1}{1 + x} \right. \\ &\quad \left. - \frac{1}{(1 + x)\Gamma(\kappa_A)} \gamma \left(\kappa_A, \sqrt{\frac{x\varpi}{\eta_A \omega_A^2}} \right) \right) dx. \end{aligned} \quad (48)$$

The integral form average achievable rate of U_A can be evaluated numerically in efficient ways. Further, a closed form approximation to (47) can be obtained as follows. By changing the integration variable of (47) as

$$t = \frac{1}{1 + x}, \quad (49)$$

we can obtain that

$$\begin{aligned} R_A &= \frac{1}{\ln(2)} \\ &\quad \times \int_0^1 \left(\frac{1}{t} - \frac{1}{t\Gamma(\kappa_A)} \gamma \left(\kappa_A, \sqrt{\frac{(1-t)(\sigma_I^2 + \sigma_T^2)}{tP_A \eta_A \omega_A^2}} \right) \right) dt \\ &\stackrel{(b)}{\approx} \frac{\pi}{K \ln(4)} \sum_{k=1}^K \sqrt{1 - \varphi_k^2} \\ &\quad \times \left(\frac{1}{b_1} - \frac{1}{b_1 \Gamma(\kappa_A)} \gamma \left(\kappa_A, \sqrt{\frac{(1-b_1)(\sigma_I^2 + \sigma_T^2)}{b_1 P_A \eta_A \omega_A^2}} \right) \right), \end{aligned} \quad (50)$$

where (b) is due to the GCQ method; φ_k and b_1 have been defined in (44a) and (44b), respectively; K is the complexity-accuracy trade-off factor, and the approximation error is negligible for large value of K .

Remark 6. If $\epsilon = 1$ and P_A is large, a closed form approximation to (48) can be given as

$$\begin{aligned} R_A &\approx \frac{\pi}{K \ln(4)} \sum_{k=1}^K \sqrt{1 - \varphi_k^2} \\ &\quad \times \left(\frac{1}{b_1} - \frac{1}{b_1 \Gamma(\kappa_A)} \gamma \left(\kappa_A, \sqrt{\frac{(1-b_1)\varpi}{b_1 \eta_A \omega_A^2}} \right) \right). \end{aligned} \quad (51)$$

2) *Average Achievable Rate of U_B :* Following the similar method, the average achievable rate of U_B can be given as

$$R_B = \frac{1}{\ln(2)} \int_0^\infty \frac{1 - \bar{P}_B(x)}{1 + x} dx, \quad (52)$$

where $\bar{P}_B(\bar{\gamma})$ is the outage probability of U_B , derived in (42). Further, a closed form approximation of R_B can be derived by using the approximation to $\bar{P}_B(\bar{\gamma})$, i.e., $\bar{P}_B^+(\bar{\gamma})$ given in (43). By changing the integration variable of (52) as

$$t = \frac{1}{1 + x}, \quad (53)$$

the average achievable rate of U_B can be transformed as

$$\begin{aligned}
R_B &= \frac{1}{\ln(2)} \int_0^1 \left(\frac{1}{t} - \frac{\bar{P}_B^+ \left(\frac{1}{t} - 1 \right)}{t} \right) dt \\
&\stackrel{(c)}{\approx} \frac{\pi}{Q \ln(4)} \sum_{q=1}^Q \sqrt{1 - \varphi_q^2} \left(\frac{1}{b_2} - \frac{\bar{P}_B^+ \left(\frac{1}{b_2} - 1 \right)}{b_2} \right) \\
&= \frac{\pi}{Q \ln(4)} \sum_{q=1}^Q \sqrt{1 - \varphi_q^2} \\
&\quad \times \left(\frac{1}{b_2} - \frac{\pi}{2K\Gamma(\kappa_B)b_2} \sum_{k=1}^K \sqrt{1 - \varphi_k^2} \right. \\
&\quad \left. \times \gamma \left(\kappa_B, \sqrt{\frac{\left(\frac{1}{b_2} - 1 \right) \left(\frac{P_A}{\xi_I} \ln \left(\frac{1}{b_1} \right) + \sigma_B^2 \right)}{P_T \eta_B \omega_B^2}} \right) \right), \tag{54}
\end{aligned}$$

where

$$\varphi_q = \cos \left(\frac{\pi}{2Q} (2q - 1) \right), \tag{55a}$$

$$b_2 = \frac{\varphi_q}{2} + \frac{1}{2}; \tag{55b}$$

(c) is due the GCQ method; Q is the complexity-accuracy trade-off factor, and the approximation error is negligible for large value of Q .

B. Discussion on HD Communication

Since a main feature of the FD communication is the residual SI, which affects the performance of U_A , we compared the performance of U_A with the FD and HD communication schemes here. Firstly, a tight upper bound on the average achievable rate of U_A with FD communication is derived with the well-known Jensen's inequality [50], such that

$$\mathbb{E}[f(X)] \leq f(\mathbb{E}[X]), \tag{56}$$

for any random variable X and concave function $f(x)$.

With Jensen's inequality, an upper bound on the average achievable rate of U_A can be given as

$$\begin{aligned}
\hat{R}_A &= \log_2 (1 + \mathbb{E}[\gamma_A]) \\
&= \log_2 \left(1 + \frac{P_A \eta_A \mathbb{E}[H_A^2]}{\sigma_I^2 + \sigma_T^2} \right) \\
&= \log_2 \left(1 + \frac{P_A \eta_A \omega_A^2 \Gamma(\kappa_A + 2)}{(\sigma_I^2 + \sigma_T^2) \Gamma(\kappa_A)} \right) \tag{57}
\end{aligned}$$

For comparison, the performance of the HD communication scheme is introduced here. Specifically, TX serves the uplink and downlink users consecutively in two identical time slots. In the first time slot, TX receives the signal coming from U_A . And, TX transmits the signal towards U_B in the second time slot. In each time slot, the phases of the corresponding RIS are shifted to maximize the composite gain of the corresponding

channels. Therefore, the average achievable rate of U_A in the HD communication scheme can be written as

$$R_A^* = \frac{1}{2} \mathbb{E}[\log_2 (1 + \gamma_A^*)], \tag{58}$$

where

$$\gamma_A^* = \frac{P_A \eta_A H_A^2}{\sigma_T^2}. \tag{59}$$

By using Jensen's inequality, an upper bound on the average achievable rate of U_A in the HD communication scheme is given by

$$\hat{R}_A^* = \frac{1}{2} \log_2 \left(1 + \frac{P_A \eta_A \omega_A^2 \Gamma(\kappa_A + 2)}{\sigma_T^2 \Gamma(\kappa_A)} \right). \tag{60}$$

Compared (57) with (60), it can be learned that the received SINR of the uplink transmission is larger with the HD communication scheme due to the lack of SI. However, the average achievable rate of the HD communication scheme is with the penalty of a 1/2 pre-log coefficient. The superiority of FD and HD communication schemes depends on the level of the residual SI after the SI cancellation procedures. It can be derived that $\hat{R}_A > \hat{R}_A^*$ if

$$\sigma_I^2 < \sqrt{\sigma_T^4 + P_A \eta_A \omega_A^2 \sigma_T^2} \frac{\Gamma(\kappa_A + 2)}{\Gamma(\kappa_A)}. \tag{61}$$

As expected, the FD communication scheme performs better as long as the power of the residual SI is lower than the threshold given in (61).

V. NUMERICAL RESULTS

In this section, simulation results are provided to verify the effectiveness of the proposed analysis, and illustrate the impacts of different system parameters on the uplink and downlink communication performance.

A. Simulation Setup

If not otherwise stated, we set the simulation parameters for the Monte Carlo (MC) simulations as follows. For the uplink transmission, the distances of the U_A - S_A and S_A -TX links are given as $d_{h,A} = 5$ m and $d_{g,A} = 20$ m, respectively. The path loss per unit distance of the uplink channel is set to be $\Lambda_A = -20$ dB. For the downlink transmission, the distances of the TX- S_B and S_B - U_B are set as $d_{h,B} = 4$ m and $d_{g,B} = 20$ m, respectively. The path loss per unit distance of the downlink channel is $\Lambda_B = -20$ dB. This reflects the scenario where S_A and S_B are placed closed to U_A and U_B , respectively. Regarding the interference channel, the distances of the S_A - U_B and S_B - U_A links are set to be $d_{I,A} = d_{I,B} = 30$ m. The distance of the U_A - U_B link is $d_0 = 25$ m. The path loss per unit distance of the interference channels are $\Lambda_{I,A} = \Lambda_{I,B} = \Lambda_D = -25$ dB. The operating carrier frequency of the system is $f_c = 3$ GHz, thus, the wavelength is $\lambda_c = 0.1$ m. Each element is of the size $l_A = l_B = \frac{\lambda_c}{2}$, $w_A = w_B = \frac{\lambda_c}{2}$. The path loss exponent is $\chi = 3$. The AWGN noise power at TX and U_B are set to be $\sigma_T^2 = \sigma_B^2 = -70$ dBm. We generate all

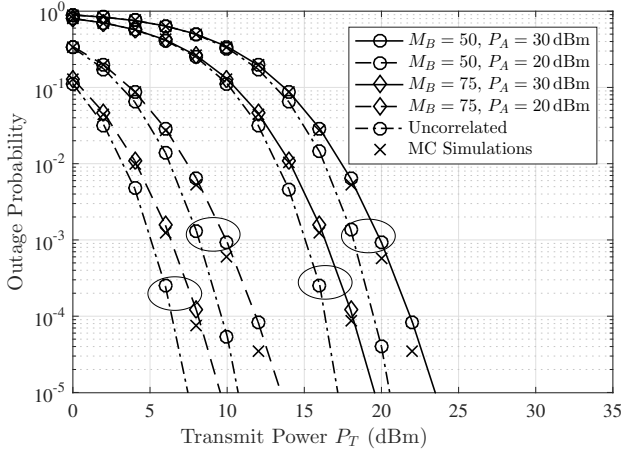


Fig. 3. Outage probability of U_B versus the transmit power with different number of elements. The curves of correlated and uncorrelated channels with same M_B and P_A are circled together.

the correlated Nakagami- m random variables in simulations by using the decomposition method proposed in [51]. The proposed analysis can be applied for any number of RIS elements. The number of RIS elements used in simulations is relatively small for clear illustrations.

B. Downlink Transmission Analysis

Fig. 3 and Fig. 4 illustrate the outage probability and average achievable rate of U_B versus the transmit power of TX. RIS elements on S_B are implemented in a rectangular array with five elements per column, i.e., $M_{v,B} = 5$. The number of elements per row varies in $M_{h,B} \in \{10, 15\}$. Hence, the number of elements on S_B varies in $M_B \in \{50, 75\}$. The element configuration of S_A is: $M_A = 50$, $M_{v,A} = 5$, $M_{h,A} = 10$. $\rho_A = \rho_B = 0.5$. The transmit power of U_A varies in $P_A \in \{20 \text{ dBm}, 30 \text{ dBm}\}$. The Nakagami- m shape parameters are set to be $a_{h,B} = a_{g,B} = 2$. As can be seen from the figures, the derived expressions match well with the simulation results. Increasing the number of elements on S_B and reducing the transmit power of U_A are both beneficial for the system performance due to the increased desired signal power and the decreased interference power, respectively. For example, when the transmit power of TX is $P_T = 15 \text{ dBm}$ and $P_A = 30 \text{ dBm}$, the average achievable rates of U_B are 3 bits/s/Hz and 4 bits/s/Hz for $M_B = 50$ and $M_B = 75$, respectively. To illustrate the impact of channel correlations on the communication performance, a benchmark that all the channels are assumed to be uncorrelated is given for comparison in Fig. 3. As expected, channel correlation has a negative impact on the system performance. For example, when the transmit power of TX is $P_T = 10 \text{ dBm}$, the number of elements on S_B is $M_B = 50$, and the transmit power of U_A is $P_A = 20 \text{ dBm}$, the outage probability is 10^{-3} and 6×10^{-5} for correlated and uncorrelated channels, respectively.

The relative error between $\bar{P}_B(\bar{\gamma})$ and its GCQ-based approximation $\bar{P}_B^+(\bar{\gamma})$ for different values of the complexity-

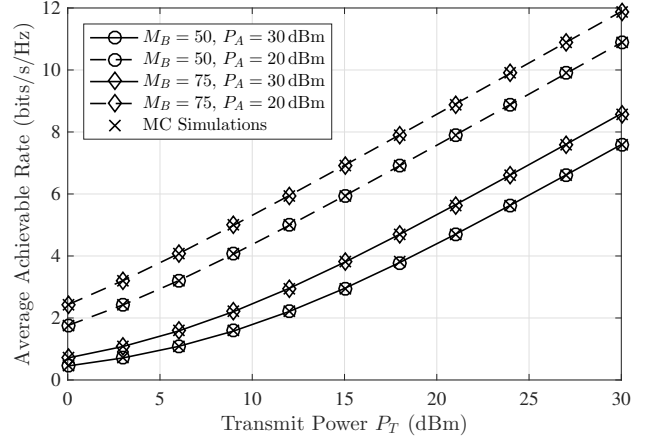


Fig. 4. Average Achievable of U_B versus the transmit power with different number of elements.

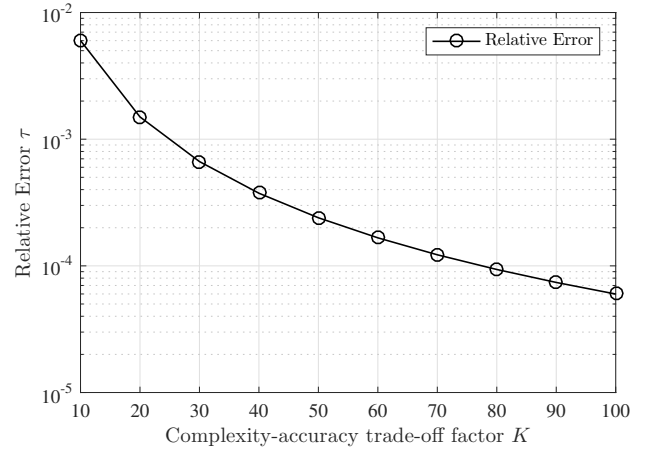


Fig. 5. Relative error of the GCQ based approximation.

accuracy trade-off factor K is presented in Fig. 5. The relative error is defined as

$$\tau = \frac{|\bar{P}_B(\bar{\gamma}) - \bar{P}_B^+(\bar{\gamma})|}{\bar{P}_B(\bar{\gamma})}. \quad (62)$$

We assume that the number of elements of S_A and S_B are as follows: $M_A = 50$, $M_{v,A} = 5$, $M_{h,A} = 10$; $M_B = 50$, $M_{v,B} = 5$, $M_{h,B} = 10$, and $\rho_A = \rho_B = 0.5$. The transmit power of U_A and TX are $P_A = 30 \text{ dBm}$ and $P_T = 10 \text{ dBm}$. Our results indicate that the GCQ-based approximation is highly accurate even for small values of K . For example, the relative error is already less than 10^{-3} when K is 30.

C. Uplink Transmission Analysis

Fig. 6 shows the outage probability of the uplink transmission versus the transmit power of U_A . RIS elements on S_A are deployed in a compact rectangular array with five elements per column, i.e., $M_{v,A} = 5$. The number of RIS elements per row varies in $M_{h,A} \in \{10, 15, 20\}$. The Nakagami- m shape parameters are set to be $a_{h,A} = a_{g,A} = 2$. $\rho_A = 0.5$. Regarding the residual SI, we set $\varpi = 10^{-7}$ and $\epsilon = 0$,

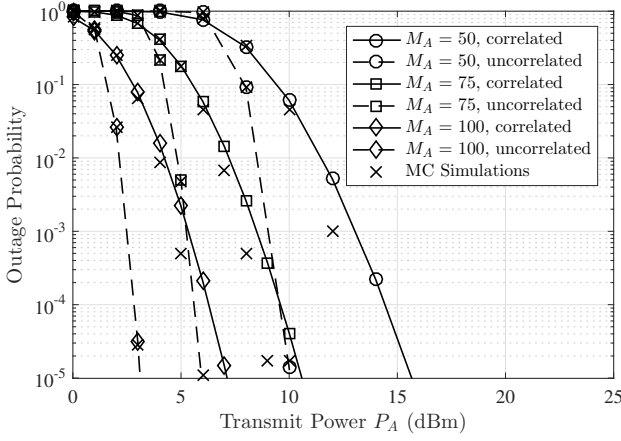


Fig. 6. Outage probability of U_A versus the transmit power with different number of elements.

representing the case where the residual SI is independent of the transmit power of TX. As illustrated in Fig. 6, increasing the number of RIS elements can improve the communication performance. In other words, the lower outage probability can be achieved with a larger number of RIS elements. For example, to achieve the outage probability of 10^{-4} with correlated channels, the required transmit power of U_A is $P_A = 8.5$ dBm and $P_A = 5.5$ dBm for $N = 75$ and $N = 100$, respectively. Same as the downlink transmission, the channel correlation effect will deteriorate the system performance. When the transmit power of U_A is $P_A = 10$ dBm and the number of elements is $M_A = 50$, the outage probability is 4×10^{-2} and 10^{-5} for correlated and uncorrelated channels, respectively. It is worth noting that the proposed gamma approximation is more accurate for the case of uncorrelated channels than the case of correlated channels, especially in the large transmit power regime. And, the approximation is more accurate for larger number of RIS elements. This is due to not only the approximation errors, but also the errors brought by the correlated Nakagami- m random variables generation method [51]. However, the proposed method in this paper already provided us with expressions in concise form, which can demonstrate the impacts of channel correlations on the system performance. The approximation gap is less than 1 dBm for the same outage probability.

Fig. 7 explores the impact of residual SI on the system performance. RIS elements on S_A are placed in a rectangular array with five elements per column and fifteen elements per row, such that $M_{v,A} = 5$ and $M_{h,A} = 15$. $\rho_A = 0.3$. The Nakagami- m shape parameters are set to be $a_{h,A} = a_{g,A} = 2$. It is assumed that the transmit power of U_A and TX are equal, i.e., $P_A = P_T$. Regarding the residual SI, we set $\varpi = 3 \times 10^{-5}$, and $\epsilon \in \{0, 0.5, 1\}$. $\epsilon = 0$ and $\epsilon = 1$ stand for the cases where the residual SI is independent and linearly dependent of the transmit power, respectively. For different residual SI exponent ϵ , it can be observed that the outage probability converges to a constant for $\epsilon = 1$, and decreases with the increase of the transmit power for $0 \leq \epsilon < 1$ in the large

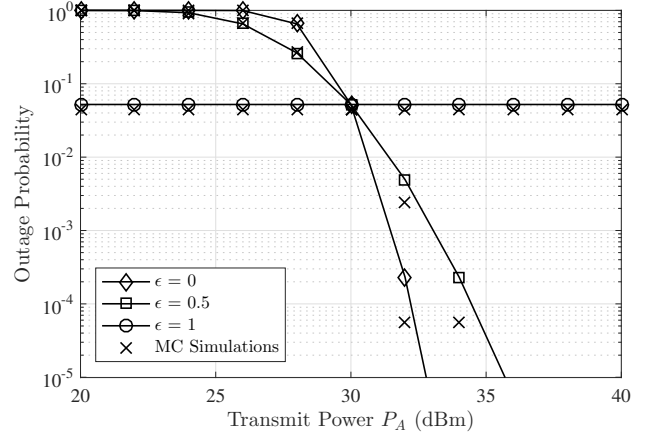


Fig. 7. Outage probability of U_A versus the transmit power with different ϵ .

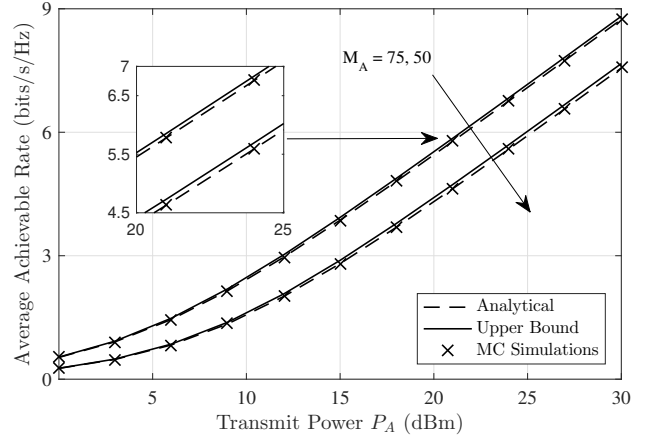


Fig. 8. Average achievable rate of U_A versus the transmit power with different number of elements.

transmit power regime. This confirms our analysis in Remark 3. Furthermore, if $0 < \epsilon < 1$, the system performance falls between the cases of $\epsilon = 0$ and $\epsilon = 1$.

Fig. 8 illustrates the average achievable rate of the uplink transmission versus the transmit power of U_A . The element configuration of S_A is $M_{v,A} = 5$, $M_{h,A} \in \{10, 15\}$, i.e., $M_A \in \{50, 75\}$. The Nakagami- m shape parameters are $a_{h,A} = a_{g,A} = 2$. $\rho_A = 0.5$. The residual SI coefficient and exponent are given as $\varpi = 10^{-7}$ and $\epsilon = 0$, respectively. In the legend, ‘Analytical’ and ‘Upper Bound’ stand for average achievable rate derived from the outage probability expression in (47) and the upper bound derived in (57), respectively. As can be seen from Fig. 8, the analytical results exactly match with the simulation results, and the upper bounds are also very tight. Similar to the outage probability, increasing the number of elements will improve the average achievable rate. For example, when $P_A = 15$ dBm, the average achievable rates are $R_A = 2.8$ bits/s/Hz and $R_A = 3.9$ bits/s/Hz for $M_A = 50$ and $M_A = 75$, respectively.

Fig. 9 demonstrates the impact of the residual SI on the system performance by illustrating the average achievable

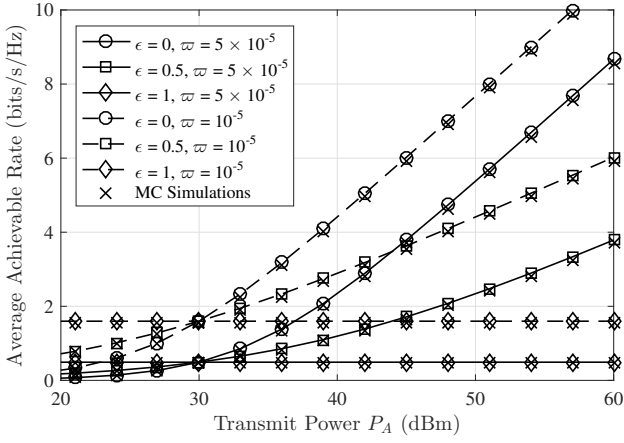


Fig. 9. Average achievable rate of U_A versus the transmit power with different ϵ .

rate versus the transmit power of U_A where the residual SI coefficient and exponent vary in $\varpi \in \{10^{-5}, 5 \times 10^{-5}\}$ and $\epsilon \in \{0, 0.5, 1\}$. We set $a_{h,A} = a_{g,A} = 2$; $\rho_A = 0.5$; $P_A = P_T$. RIS elements on S_A are deployed with $M_{v,A} = 5$ elements per column and $M_{h,A} = 10$ elements per column. As shown in the figure, smaller residual SI coefficient ϖ will lead to higher average achievable rate. For example, when $P_A = 45$ dBm and $\epsilon = 0$, the average achievable rates of U_A are 6 bits/s/Hz and 3.7 bits/s/Hz for $\varpi = 10^{-5}$ and $\varpi = 5 \times 10^{-5}$, respectively. Further, similar to the case of the outage probability, the average achievable rate converges to a constant value due to the linear dependence between the transmit power and the residual SI.

D. FD and HD Communications Comparison

Fig. 10 is presented to verify the boundary at which the FD communication scheme is better than the HD communication given in (61). The element configuration of S_A is $M_A = 50$, $M_{v,A} = 5$, $M_{h,A} = 10$. The transmit power of U_A varies in $P_A \in \{20 \text{ dBm}, 30 \text{ dBm}\}$. The residual SI lies in $\sigma_l^2 \in (-70 \text{ dBm}, -20 \text{ dBm})$. The average achievable rate of the HD communication is a constant since the residual SI does not exist in the HD mode. As can be seen from Fig. 10, the FD communication outperforms the HD communication when the residual SI is lower than a threshold value. The boundary given by (61) is very precise as proven by the simulations.

VI. CONCLUSIONS

This paper study a RIS-assisted FD communication network, where an uplink user and a downlink user are served by an FD transceiver over the same time and frequency resource block. Due to the size and placement of RIS reflecting elements, the proposed system incorporates a spatially correlated Nakagami- m fading channel model. Since the exact performance analysis is mathematically intractable, we apply the moment-matching method to approximate the signal power as a gamma random variable. Then, the outage probability and the average achievable rates of the uplink and downlink users

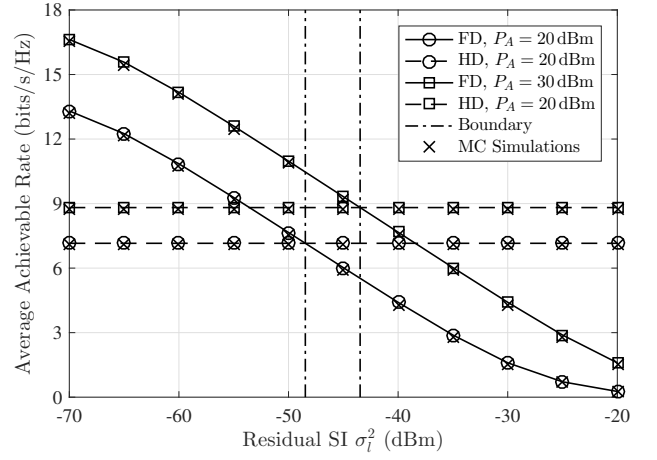


Fig. 10. FD and HD Communications Comparison.

are derived in closed form. The impact of the residual SI is explored. Floors of outage probability and average achievable rate can appear due to the linear relationship between the transmit power and the residual SI. Furthermore, the residual SI threshold below which the FD communication performs better than the HD counterpart is given in the closed form and verified by simulations.

APPENDIX A

The mean of H_u , $u \in \{A, B\}$ is calculated directly as

$$\begin{aligned} \mathbb{E}[H_u] &= \sum_{m=1}^{M_u} \mathbb{E}[|h_{m,u}|] \mathbb{E}[|g_{m,u}|] \\ &= M_u \frac{\Gamma(a_{h,u} + \frac{1}{2}) \Gamma(a_{g,u} + \frac{1}{2})}{\Gamma(a_{h,u}) \Gamma(a_{g,u})} \left(\frac{1}{a_{h,u} a_{g,u}} \right)^{\frac{1}{2}}. \end{aligned} \quad (\text{A.1})$$

The variance of H_u is the difference between the second order raw moment of H_u and the square of the mean of H_u , where the second order raw moment of H_u can be decomposed as

$$\begin{aligned} \mathbb{E}[H_u^2] &= \mathbb{E} \left[\sum_{m=1}^{M_u} |h_{m,u}|^2 |g_{m,u}|^2 \right] \\ &\quad + 2 \mathbb{E} \left[\sum_{m=1}^{M_u-1} \sum_{n=m+1}^{M_u} |h_{m,u}| |g_{m,u}| |h_{n,u}| |g_{n,u}| \right] \\ &= M_u + 2 \mathbb{E} \left[\sum_{m=1}^{M_u-1} \sum_{n=m+1}^{M_u} |h_{m,u}| |g_{m,u}| |h_{n,u}| |g_{n,u}| \right]. \end{aligned} \quad (\text{A.2})$$

The key problem lies in characterizing the mean of $|h_{m,u}| |h_{n,u}|$ and $|g_{m,u}| |g_{n,u}|$, where $m \neq n$. $|h_{m,u}|$ and

$|h_{m,u}|$ are two correlated Nakagami- m random variables such that

$$|h_{m,u}| \sim \text{Nakagami}(a_{h,u}, 1), \quad (\text{A.3a})$$

$$|h_{n,u}| \sim \text{Nakagami}(a_{h,u}, 1), \quad (\text{A.3b})$$

$$\frac{\text{Cov}(|h_{m,u}|^2, |h_{n,u}|^2)}{\sqrt{\text{Var}(|h_{m,u}|^2) \text{Var}(|h_{n,u}|^2)}} = \rho_{m,n,u}. \quad (\text{A.3c})$$

Denoting $|h_{m,u}|^2$ and $|h_{n,u}|^2$ as $H_{m,u}$ and $H_{n,u}$ respectively, and using the property of Nakagami- m distribution, $H_{m,u}$ and $H_{n,u}$ can be written as the sum of squares of independent Rayleigh random variables as

$$\begin{aligned} H_{m,u} &= \sum_{j=1}^{a_{h,u}} R_{j,m,u}^2 \\ &= R_{1,m,u}^2 + R_{2,m,u}^2 + \dots + R_{a_{h,u},m,u}^2, \end{aligned} \quad (\text{A.4a})$$

$$\begin{aligned} H_{n,u} &= \sum_{j=1}^{a_{h,u}} R_{j,n,u}^2 \\ &= R_{1,n,u}^2 + R_{2,n,u}^2 + \dots + R_{a_{h,u},n,u}^2, \end{aligned} \quad (\text{A.4b})$$

where

$$R_{a,m,u} \sim \mathcal{R}\left(\frac{1}{\sqrt{2a_{h,u}}}\right), \quad (\text{A.5a})$$

$$R_{a,n,u} \sim \mathcal{R}\left(\frac{1}{\sqrt{2a_{h,u}}}\right), \quad (\text{A.5b})$$

$$a \in \{1, 2, \dots, a_{h,u}\}, \quad (\text{A.5c})$$

$$\begin{cases} \frac{\text{Cov}(R_{a,m,u}^2, R_{a',n,u}^2)}{\sqrt{\text{Var}(R_{a,m,u}^2) \text{Var}(R_{a',n,u}^2)}} = \rho_{m,n,u}, & a = a', \\ \frac{\text{Cov}(R_{a,m,u}^2, R_{a',n,u}^2)}{\sqrt{\text{Var}(R_{a,m,u}^2) \text{Var}(R_{a',n,u}^2)}} = 0 & a \neq a', \end{cases} \quad (\text{A.6})$$

such that

$$\text{Cov}(H_{m,u}, H_{n,u}) = a_{h,u} \text{Cov}(R_{a,m,u}^2, R_{a,n,u}^2), \quad (\text{A.7a})$$

$$\begin{aligned} \text{Var}(H_{m,u}) &= \text{Var}(H_{n,u}) \\ &= a_{h,u} \text{Var}(R_{a,m,u}^2) \\ &= a_{h,u} \text{Var}(R_{a,n,u}^2). \end{aligned} \quad (\text{A.7b})$$

Following the discussion in [52], the joint distribution of $(R_{a,m,u}, R_{a,n,u})$ can be given as

$$\begin{aligned} f_{R_{a,m,u}, R_{a,n,u}}(x, y) &= \frac{4a_{h,u}^2 xy}{(1 - \rho_{m,n,u})} \exp\left(-\frac{a_{h,u}(x^2 + y^2)}{(1 - \rho_{m,n,u})}\right) \\ &\times I_0\left(\frac{2a_{h,u}\sqrt{\rho_{m,n,u}}xy}{(1 - \rho_{m,n,u})}\right). \end{aligned} \quad (\text{A.8})$$

Applying the transformation of variables, the joint distribution of $(R_{a,m,u}^2, R_{a,n,u}^2)$ can be directly obtained as

$$\begin{aligned} f_{R_{a,m,u}^2, R_{a,n,u}^2}(x, y) &= \frac{a_{h,u}^2}{(1 - \rho_{m,n,u})} \exp\left(-\frac{a_{h,u}(x + y)}{(1 - \rho_{m,n,u})}\right) \\ &\times I_0\left(\frac{2a_{h,u}\sqrt{\rho_{m,n,u}}xy}{(1 - \rho_{m,n,u})}\right) \end{aligned} \quad (\text{A.9})$$

Further, the two dimensional Laplace transform of $(R_{a,m,u}^2, R_{a,n,u}^2)$ is derived as follows:

$$\begin{aligned} \psi_{R_{a,m,u}^2, R_{a,n,u}^2}(s_1, s_2) &= \int_0^\infty \int_0^\infty e^{-s_1 x - s_2 y} f_{R_{a,m,u}^2, R_{a,n,u}^2}(x, y) dx dy \\ &= \frac{a_{h,u}^2}{(1 - \rho_{m,n,u})} \left(\left(s_1 + \frac{a_{h,u}}{1 - \rho_{m,n,u}} \right) \right. \\ &\quad \times \left. \left(s_2 + \frac{a_{h,u}}{1 - \rho_{m,n,u}} \right) - \frac{a_{h,u}^2 \rho_{m,n,u}}{(1 - \rho_{m,n,u})^2} \right)^{-1} \end{aligned} \quad (\text{A.10})$$

With the property of Laplace transform, the two dimensional Laplace transform of $(H_{m,u}, H_{n,u})$ is

$$\begin{aligned} \psi_{H_{m,u}, H_{n,u}}(s_1, s_2) &= \left(\psi_{R_{a,m,u}^2, R_{a,n,u}^2}(s_1, s_2) \right)^{a_{h,u}} \\ &= \left(\frac{a_{h,u}^2}{(1 - \rho_{m,n,u})} \right)^{a_{h,u}} \left(\left(s_1 + \frac{a_{h,u}}{1 - \rho_{m,n,u}} \right) \right. \\ &\quad \times \left. \left(s_2 + \frac{a_{h,u}}{1 - \rho_{m,n,u}} \right) - \frac{a_{h,u}^2 \rho_{m,n,u}}{(1 - \rho_{m,n,u})^2} \right)^{-a_{h,u}} \end{aligned} \quad (\text{A.11})$$

Taking the inverse two dimensional Laplace transform [53], the joint distribution of $(H_{m,u}, H_{n,u})$ is derived as

$$\begin{aligned} f_{H_{m,u}, H_{n,u}}(x, y) &= \frac{1}{(j2\pi)^2} \int_{c_1 - \infty}^{c_1 + \infty} \int_{c_2 - \infty}^{c_2 + \infty} e^{s_1 x + s_2 y} \psi_{H_{m,u}, H_{n,u}}(s_1, s_2) ds_2 ds_1 \\ &= \left(\frac{a_{h,u}^2}{(1 - \rho_{m,n,u})} \right)^{a_{h,u}} \frac{(xy)^{\frac{a_{h,u}-1}{2}} (1 - \rho_{m,n,u})^{(a_{h,u}-1)}}{\Gamma(a_{h,u}) (\sqrt{\rho_{m,n,u}} a_{h,u})^{(a_{h,u}-1)}} \\ &\times \exp\left(-\frac{a_{h,u}}{(1 - \rho_{m,n,u})}(x + y)\right) \\ &\times I_{a_{h,u}-1}\left(\frac{2\sqrt{\rho_{m,n,u}} a_{h,u}}{1 - \rho_{m,n,u}} \sqrt{xy}\right) \end{aligned} \quad (\text{A.12})$$

$\psi_{H_{m,u}, H_{n,u}}(s_1, s_2)$ is an analytic function for all s_1 and s_2 in a region confined by $\text{Re}(s_1) \geq c_1$ and $\text{Re}(s_2) \geq c_2$, where c_1 and c_2 are real constants chosen properly. Applying the transformation of variables again leads to the joint distribution of $(|h_{m,u}|, |h_{n,u}|)$ such that

$$\begin{aligned} f_{|h_{m,u}|, |h_{n,u}|}(x, y) &= \frac{4(xy)^{a_{h,u}} a_{h,u}^{(a_{h,u}+1)}}{\Gamma(a_{h,u}) (1 - \rho_{m,n,u})^{\frac{a_{h,u}-1}{2}}} \\ &\times \exp\left(-\frac{a_{h,u}}{(1 - \rho_{m,n,u})}(x^2 + y^2)\right) \\ &\times I_{a_{h,u}-1}\left(\frac{2\sqrt{\rho_{m,n,u}} a_{h,u}}{1 - \rho_{m,n,u}} xy\right). \end{aligned} \quad (\text{A.13})$$

As per the joint distribution of $(|h_{m,u}|, |h_{n,u}|)$, the mean of $|h_{m,u}| |h_{n,u}|$ can be computed as

$$\begin{aligned}\mathbb{E}[|h_{m,u}| |h_{n,u}|] &= \int_0^\infty \int_0^\infty xy f_{|h_{m,u}|, |h_{n,u}|}(x, y) dx dy \\ &= \frac{\Gamma^2(a_{h,u} + \frac{1}{2})}{a_{h,u} \Gamma^2(a_{h,u})} {}_2F_1\left(-\frac{1}{2}, -\frac{1}{2}, a_{h,u}, \rho_{m,n,u}\right).\end{aligned}\quad (\text{A.14})$$

Following the similar procedures, we can obtain the mean of $|g_{m,u}| |g_{n,u}|$ as

$$\mathbb{E}[|g_{m,u}| |g_{n,u}|] = \frac{\Gamma^2(a_{g,u} + \frac{1}{2})}{a_{g,u} \Gamma^2(a_{g,u})} {}_2F_1\left(-\frac{1}{2}, -\frac{1}{2}, a_{g,u}, \rho_{m,n,u}\right).\quad (\text{A.15})$$

Defining matrices $\mathbf{R}_{h,u}$ and $\mathbf{R}_{g,u}$ as in (25a) and (25b), we can arrive at the variance of H_u in a form as given in (23b).

APPENDIX B

As stated in (22), the average achievable rate of U_u can be rewritten as

$$\begin{aligned}R_u &\stackrel{(a)}{=} \int_0^\infty \log_2(1 + \bar{\gamma}) \frac{\partial \bar{P}_u(\bar{\gamma})}{\partial \bar{\gamma}} d\bar{\gamma} \\ &= \frac{1}{\ln(2)} \int_0^\infty \int_0^{\bar{\gamma}} \frac{1}{1+x} dx \frac{\partial \bar{P}_u(\bar{\gamma})}{\partial \bar{\gamma}} d\bar{\gamma} \\ &\stackrel{(b)}{=} \frac{1}{\ln(2)} \int_0^\infty \frac{1}{1+x} \int_x^\infty \frac{\bar{P}_u(\bar{\gamma})}{\partial \bar{\gamma}} d\bar{\gamma} dx \\ &= \frac{1}{\ln(2)} \int_0^\infty \frac{1 - \bar{P}_u(x)}{1+x} dx,\end{aligned}\quad (\text{B.1})$$

where (a) is obtained by using the relationship between the CDF and PDF of a random variable; (b) is derived by exchanging the order of integration.

REFERENCES

- [1] S. Dang, O. Amin *et al.*, "What should 6G be?" *Nat. Electron.*, vol. 3, no. 1, pp. 20–29, 2020.
- [2] F. Rusek, D. Persson *et al.*, "Scaling up MIMO: Opportunities and challenges with very large arrays," *IEEE Signal Process. Mag.*, vol. 30, no. 1, pp. 40–60, 2012.
- [3] S. Han, I. Chih-Lin *et al.*, "Large-scale antenna systems with hybrid analog and digital beamforming for millimeter wave 5G," *IEEE Commun. Mag.*, vol. 53, no. 1, pp. 186–194, 2015.
- [4] P. Popovski, Č. Stefanović *et al.*, "Wireless access in ultra-reliable low-latency communication (URLLC)," *IEEE Trans. Commun.*, vol. 67, no. 8, pp. 5783–5801, 2019.
- [5] N. Bhushan, J. Li *et al.*, "Network densification: the dominant theme for wireless evolution into 5G," *IEEE Commun. Mag.*, vol. 52, no. 2, pp. 82–89, 2014.
- [6] Q. Wu, S. Zhang *et al.*, "Intelligent reflecting surface-aided wireless communications: A tutorial," *IEEE Trans. Commun.*, vol. 69, no. 5, pp. 3313–3351, 2021.
- [7] Q. Wu and R. Zhang, "Intelligent reflecting surface enhanced wireless network via joint active and passive beamforming," *IEEE Trans. Wireless Commun.*, vol. 18, no. 11, pp. 5394–5409, 2019.
- [8] C. Pan, H. Ren *et al.*, "Reconfigurable intelligent surfaces for 6G systems: Principles, applications, and research directions," *IEEE Commun. Mag.*, vol. 59, no. 6, pp. 14–20, 2021.
- [9] C. Liaskos, S. Nie *et al.*, "A new wireless communication paradigm through software-controlled metasurfaces," *IEEE Commun. Mag.*, vol. 56, no. 9, pp. 162–169, 2018.
- [10] Y. Yang, B. Zheng *et al.*, "Intelligent reflecting surface meets OFDM: Protocol design and rate maximization," *IEEE Trans. Commun.*, vol. 68, no. 7, pp. 4522–4535, 2020.
- [11] T. Hou, Y. Liu *et al.*, "Reconfigurable intelligent surface aided NOMA networks," *IEEE J. Sel. Areas Commun.*, vol. 38, no. 11, pp. 2575–2588, 2020.
- [12] P. Xu, G. Chen *et al.*, "Ergodic secrecy rate of RIS-assisted communication systems in the presence of discrete phase shifts and multiple eavesdroppers," *IEEE Wireless Commun. Lett.*, vol. 10, no. 3, pp. 629–633, 2021.
- [13] X. Pang, M. Sheng *et al.*, "When UAV meets IRS: Expanding air-ground networks via passive reflection," *IEEE Wireless Commun.*, vol. 28, no. 5, pp. 164–170, 2021.
- [14] Ö. Özdoğan, E. Björnson, and E. G. Larsson, "Intelligent reflecting surfaces: Physics, propagation, and pathloss modeling," *IEEE Wireless Commun. Lett.*, vol. 9, no. 5, pp. 581–585, 2019.
- [15] D. Kudathanthirige, D. Gunasinghe, and G. Amarasinguriya, "Performance analysis of intelligent reflective surfaces for wireless communication," in *Proc. IEEE Int. Conf. Commun. (ICC)*, Dublin, Ireland, Jun. 2020, pp. 1–6.
- [16] D. Li, "Ergodic capacity of intelligent reflecting surface-assisted communication systems with phase errors," *IEEE Commun. Lett.*, vol. 24, no. 8, pp. 1646–1650, 2020.
- [17] T. Wang, G. Chen *et al.*, "Study of intelligent reflective surface assisted communications with one-bit phase adjustments," in *Proc. IEEE Global Commun. Conf. (GLOBECOM)*, Virtual, Dec. 2020, pp. 1–6.
- [18] M. Badiu and J. P. Coon, "Communication through a large reflecting surface with phase errors," *IEEE Wireless Commun. Lett.*, vol. 9, no. 2, pp. 184–188, 2020.
- [19] Q. Tao, J. Wang, and C. Zhong, "Performance analysis of intelligent reflecting surface aided communication systems," *IEEE Commun. Lett.*, vol. 24, no. 11, pp. 2464–2468, 2020.
- [20] A. M. Salhab and M. H. Samuh, "Accurate performance analysis of reconfigurable intelligent surfaces over Rician fading channels," *IEEE Wireless Commun. Lett.*, vol. 10, no. 5, pp. 1051–1055, 2021.
- [21] H. Zhang, B. Di *et al.*, "Reconfigurable intelligent surfaces assisted communications with limited phase shifts: How many phase shifts are enough?" *IEEE Trans. Veh. Technol.*, vol. 69, no. 4, pp. 4498–4502, 2020.
- [22] R. C. Ferreira, M. S. Facina *et al.*, "Bit error probability for large intelligent surfaces under double-Nakagami fading channels," *IEEE Open J. Commun. Soc.*, vol. 1, pp. 750–759, 2020.
- [23] H. Ibrahim, H. Tabassum, and U. T. Nguyen, "Exact coverage analysis of intelligent reflecting surfaces with Nakagami-m channels," *IEEE Trans. Veh. Technol.*, vol. 70, no. 1, pp. 1072–1076, 2021.
- [24] E. Björnson and L. Sanguinetti, "Rayleigh fading modeling and channel hardening for reconfigurable intelligent surfaces," *IEEE Wireless Commun. Lett.*, vol. 10, no. 4, pp. 830–834, 2020.
- [25] T. Wang, M.-A. Badiu *et al.*, "Outage probability analysis of STAR-RIS assisted NOMA network with correlated channels," *IEEE Commun. Lett.*, 2022, Early Access.
- [26] T. Van Chien, A. K. Papazafeiropoulos *et al.*, "Outage probability analysis of IRS-assisted systems under spatially correlated channels," *IEEE Wireless Commun. Lett.*, vol. 10, no. 8, pp. 1815–1819, 2021.
- [27] T. Wang, M.-A. Badiu *et al.*, "Performance analysis of IOS-assisted NOMA system with channel correlation and phase errors," *IEEE Trans. Veh. Technol.*, vol. 71, no. 11, pp. 11 861–11 875, 2022.
- [28] I. Trigui, W. Ajib, and W.-P. Zhu, "Reconfigurable intelligent surfaces-aided relaying in correlated Rice fading: Performance analysis and design optimization," *IEEE Trans. Veh. Technol.*, 2022, Early Access.
- [29] I. Singh, P. J. Smith, and P. A. Dmochowski, "Optimal SNR analysis for single-user RIS systems in Rician and Rayleigh environments," *IEEE Trans. Wireless Commun.*, 2022.
- [30] Y. Zhang, C. Zhong *et al.*, "Sum rate optimization for two way communications with intelligent reflecting surface," *IEEE Commun. Lett.*, vol. 24, no. 5, pp. 1090–1094, 2020.
- [31] S. Atapattu, R. Fan *et al.*, "Reconfigurable intelligent surface assisted two-way communications: Performance analysis and optimization," *IEEE Trans. Wireless Commun.*, vol. 68, no. 10, pp. 6552–6567, 2020.
- [32] Y. Cai, M.-M. Zhao *et al.*, "Intelligent reflecting surface aided full-duplex communication: Passive beamforming and deployment design," *IEEE Trans. Wireless Commun.*, vol. 21, no. 1, pp. 383–397, 2021.
- [33] K. Singh, F. Karim *et al.*, "Performance analysis of RIS-assisted full-duplex communications with infinite and finite blocklength codes," *IEEE Trans. Commun.*, 2023, Early Access.

- [34] A. M. T. Khel and K. A. Hamdi, "Performance analysis of IRS-assisted full-duplex wireless communication systems with interference," *IEEE Commun. Lett.*, vol. 26, no. 9, pp. 2027–2031, 2022.
- [35] T.-H. Vu and S. Kim, "Performance analysis of full-duplex two-way RIS-based systems with imperfect CSI and discrete phase-shift design," *IEEE Commun. Lett.*, 2022.
- [36] P. K. Sharma and P. Garg, "Intelligent reflecting surfaces to achieve the full-duplex wireless communication," *IEEE Commun. Lett.*, vol. 25, no. 2, pp. 622–626, 2020.
- [37] S. Dhok and P. K. Sharma, "Infinite and finite block-length FD transmissions with spatially-correlated RIS channels," *IEEE Trans. Wireless Commun.*, 2022, Early Access.
- [38] J. Lyu and R. Zhang, "Hybrid active/passive wireless network aided by intelligent reflecting surface: System modeling and performance analysis," *IEEE Trans. Wireless Commun.*, vol. 20, no. 11, pp. 7196–7212, 2021.
- [39] A. Goldsmith, *Wireless communications*. Cambridge university press, 2005.
- [40] G. K. Karagiannidis, D. A. Zogas, and S. A. Kotsopoulos, "Performance analysis of triple selection diversity over exponentially correlated Nakagami-m fading channels," *IEEE Trans. Commun.*, vol. 51, no. 8, pp. 1245–1248, 2003.
- [41] P. Sahu and A. K. Chaturvedi, "Performance analysis of predetection EGC in exponentially correlated nakagami-m fading channel," *IEEE trans. commun.*, vol. 53, no. 8, pp. 1252–1256, 2005.
- [42] G. K. Karagiannidis, D. A. Zogas, and S. A. Kotsopoulos, "On the multivariate Nakagami-m distribution with exponential correlation," *IEEE Trans. Commun.*, vol. 51, no. 8, pp. 1240–1244, 2003.
- [43] C. Zhang, W. Yi *et al.*, "Reconfigurable intelligent surfaces aided multi-cell NOMA networks: A stochastic geometry model," *IEEE Trans. Commun.*, vol. 70, no. 2, pp. 951–966, 2022.
- [44] S. Atapattu, P. Dharmawansa *et al.*, "Multi-user relay selection for full-duplex radio," *IEEE Trans. Commun.*, vol. 67, no. 2, pp. 955–972, 2018.
- [45] A. Sabharwal, P. Schniter *et al.*, "In-band full-duplex wireless: Challenges and opportunities," *IEEE J. Sel. Areas Commun.*, vol. 32, no. 9, pp. 1637–1652, 2014.
- [46] L. J. Rodriguez, N. H. Tran, and T. Le-Ngoc, "Performance of full-duplex AF relaying in the presence of residual self-interference," *IEEE J. Sel. Areas Commun.*, vol. 32, no. 9, pp. 1752–1764, 2014.
- [47] S. Atapattu, C. Tellambura, and H. Jiang, "A mixture gamma distribution to model the SNR of wireless channels," *IEEE Trans. Wireless Commun.*, vol. 10, no. 12, pp. 4193–4203, 2011.
- [48] V. A. Aalo, "Performance of maximal-ratio diversity systems in a correlated Nakagami-fading environment," *IEEE Trans. Commun.*, vol. 43, no. 8, pp. 2360–2369, 1995.
- [49] M. Abramowitz and I. A. Stegun, *Handbook of mathematical functions with formulas, graphs, and mathematical tables*. US Government printing office, 1964, vol. 55.
- [50] S. Boyd and L. Vandenberghe, *Convex Optimization*. Cambridge university press, 2004.
- [51] Q. Zhang, "A decomposition technique for efficient generation of correlated Nakagami fading channels," *IEEE J. Sel. Areas Commun.*, vol. 18, no. 11, pp. 2385–2392, 2000.
- [52] M. Nakagami, "The m-distribution—a general formula of intensity distribution of rapid fading," in *Statistical methods in radio wave propagation*. Elsevier, 1960, pp. 3–36.
- [53] L. Debnath, "The double laplace transforms and their properties with applications to functional, integral and partial differential equations," *Int. J. Appl. Comput. Math.*, vol. 2, no. 2, pp. 223–241, 2016.



Tianxiong Wang received the B.Sc. degree in electronic science and technology from the Beijing Institute of Technology, China, in 2019, and the Ph.D. degree in communications from the Department of Engineering Science, University of Oxford, U.K., in 2023. He is currently with the Future Research Laboratory, China Mobile Research Institute. His research interests are in the fields of reconfigurable intelligent surface (RIS), performance analysis, non-orthogonal multiple access (NOMA), stochastic geometry, and wireless communications. He received the Exemplary Reviewer Award of the IEEE COMMUNICATIONS LETTERS in 2022. He serves as a reviewer for the IEEE COMMUNICATIONS LETTERS, IEEE WIRELESS COMMUNICATIONS LETTERS, and IEEE TRANSACTIONS ON WIRELESS COMMUNICATIONS.



Gaojie Chen (S'09 – M'12 – SM'18) received the B.Eng. and B.Ec. Degrees in electrical information engineering and international economics and trade from Northwest University, China, in 2006, and the M.Sc. (Hons.) and PhD degrees in electrical and electronic engineering from Loughborough University, Loughborough, U.K., in 2008 and 2012, respectively. After graduation, he took up academic and research positions at DT Mobile, Loughborough University, University of Surrey, University of Oxford and University of Leicester, U.K. He is currently an Assistant Professor with the Institute for Communication Systems, 5GIC & 6GIC, University of Surrey, U.K., and a Visiting Research Collaborator with the Information and Network Science Lab, University of Oxford, U.K. His current research interests include information theory, wireless communications, satellite communications, cognitive radio, the Internet of Things, secrecy communications, and random geometric networks. He received the Exemplary Reviewer Awards of the IEEE WIRELESS COMMUNICATIONS LETTERS in 2018, the IEEE TRANSACTIONS ON COMMUNICATIONS in 2019 and the IEEE COMMUNICATIONS LETTERS in 2020 and 2021; and Exemplary Editor Awards of the IEEE COMMUNICATIONS LETTERS and IEEE WIRELESS COMMUNICATIONS LETTERS in 2021 and 2022, respectively. He served as an Associate Editor for the IEEE JOURNAL ON SELECTED AREAS IN COMMUNICATIONS - Machine Learning in Communications from 2021–2022. He serves as an Associate Editor for the IEEE TRANSACTIONS ON WIRELESS COMMUNICATIONS, the IEEE COMMUNICATIONS LETTERS and IEEE WIRELESS COMMUNICATIONS LETTERS.



Justin P. Coon (Senior Member, IEEE) received the B.Sc. degree (with distinction) in electrical engineering from Calhoun Honours College, Clemson University, Clemson, SC, USA, in 2000 and the Ph.D. degree in communications from the University of Bristol, Bristol, U.K., in 2005. He held various research positions with Toshiba Research Europe Ltd. (TREL) from 2004 to 2013, including the position of a Research Manager from 2010 to 2013, during which, he led all research on physical layer communications and network science with TREL. He was a Visiting Fellow with the School of Mathematics, University of Bristol, from 2010 to 2012, and was a Reader with the Department of Electrical and Electronic Engineering from 2012 to 2013. In 2013, he joined the University of Oxford, Oxford, U.K., where he is currently a Professor of Engineering Science and the Emmott Fellow in Engineering Science with Oriel College, Oxford, U.K. He has authored or coauthored more than 200 papers in IEEE and APS journals and conferences and is a named Inventor on more than 30 patents. He was the recipient of the Toshiba's Distinguished Research Award for his work on 4G systems and three best paper awards. He was the Editor of several IEEE journals and has Chaired or Co-chaired various conferences. He is a Fellow of the Institute for Mathematics and its Applications.